360
12-3-79

DR. 374

SAN-2207-T3

THIN FILM POLYCRYSTALLINE SILICON SOLAR CELLS

Quarterly Report No. 2, January 1—March 30, 1979

MASTER

By
K. R. Sarma
M. J. Rice
R. Legge
W. C. Ramsey

Work Performed Under Contract No. ET-78-C-03-2207

Motorola, Inc.
Solar Energy Department
Phoenix, Arizona

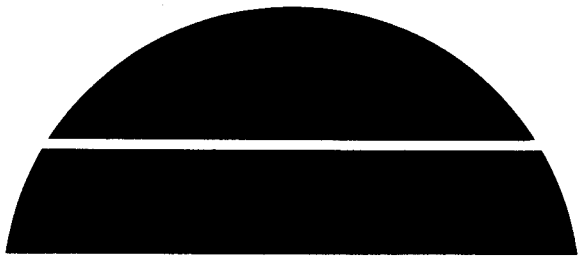

U.S. Department of Energy

Solar Energy

SAN-2207-T3
Distribution Category UC-63e

THIN FILM POLYCRYSTALLINE SILICON SOLAR CELLS

QUARTERLY REPORT NO. 2

1 JANUARY 1979 - 30 MARCH 1979

PREPARED FOR

UNITED STATES DEPARTMENT OF ENERGY

DIVISION OF SOLAR TECHNOLOGY

600 E STREET, N.W.
WASHINGTON, D.C. 20545

PREPARED BY

K.R. SARMA, M.J. RICE, R. LEGGE, W.C. RAMSEY
OF
MOTOROLA, INC.
SOLAR ENERGY DEPARTMENT
5005 EAST MCDOWELL ROAD
PHOENIX, ARIZONA 85008

MOTOROLA PROJECT NO. 2361

DOE CONTRACT NO. ET-78-C-03-2207

PREFACE

This Quarterly Report No. 2, covering the period January 1, 1979 to March 30, 1979, was prepared by the Solar Energy R&D Department, I. A. Lesk, Manager, Motorola Inc., Phoenix, Arizona 85008. The report describes the work performed under DOE Contract No. ET-78-C-93-2207. K. R. Sarma is the principal investigator. Others who participated in this program are R. W. Gurtler, M. J. Rice, A. Baghdadi, R. Legge, B. Sopori, and W. C. Ramsey.

ABSTRACT

During this quarter, a composite substrate concept was developed and shear separation successfully demonstrated. This substrate consists of a main molybdenum substrate, a thin (~ 1 μm) SiO_2 barrier layer and a thin (≈3000Å) Mo layer. The thin Mo layer gets converted to $MoSi_2$ and acts as a shear separation layer. This composite substrate shows promise for substantial improvement in recyclability and the quality of silicon ribbons produced.

Effects of $SiHCl_3$ concentration, total reactant flow rate, beam RF power, substrate temperature and gravity on energy beam deposition were investigated. The deposition efficiency was found to be a strong function of input chlorosilane concentration. Rotating nozzle deposition was also studied. Problems were encountered in the use of the rotating nozzle due to improper impedance matching with the nozzle assembly. This required redesign of the rotating assembly to improve impedance matching.

EBD silicon ribbons were grain enhanced by RTR recrystallization and successfully gettered by a two sided phosphorous diffusion which resulted in diffusion lengths ranging upto 75 μm. Solar cells, 1 x 2 cm in area were fabricated on these silicon ribbons; they exhibited conversion efficiencies of upto 10.1% with a V_{OC} of 0.54V, J_{SC} of 29.5 mA/cm^2 and a FF of 63%.

TABLE OF CONTENTS

1.0 INTRODUCTION

The objectives of this research program are: (1) investigation of the Energy Beam as a means for efficient, high-rate deposition of polysilicon films; (2) development of temporary, reuseable substrates for polysilicon deposition; (3) development and optimization of subsequent grain enhancement of the thin silicon films through laser recrystallization; and (4) demonstration of at least 10% efficient solar cells fabricated on grain enhanced silicon films.

During this quarter we have continued investigation of diffusion barriers and developed and demonstrated a composite substrate concept. Composite substrates show the promise for both increased substrate recyclability and improved silicon film quality (chemical purity).

Parametric studies of Energy Beam Deposition (EBD) were continued. Whisker and nodule growth in EBD were investigated. Rotating nozzle deposition was also studied.

EBD silicon ribbons were grain enhanced and successfully gettered by a two sided phosphorous diffusion process to obtain minority carrier diffusion lengths (as measured by SPV) ranging up to 75 μm. Solar cells have been fabricated on the gettered silicon ribbons. Conversion efficiencies up to 10.1% have been observed in these cells.

2.0 SUBSTRATE SYSTEM STUDIES

To prevent continued growth of a $MoSi_2$ layer on the Mo substrate, and also to minimize possible contamination from metallurgical grade Mo substrates, various diffusion barriers have been examined for their effectiveness. We have reported [1] that SiO_2 is very effective as a diffusion barrier for Mo and Si, and prevents the formation of a $MoSi_2$ layer. However, deposited silicon films were found to be adherent to the SiO_2 coated Mo substrates, indicating the necessity of a $MoSi_2$ shear separation layer. During this quarter, a composite substrate concept was developed and successfully demonstrated.

2.1 COMPOSITE SUBSTRATES

By employing a composite substrate with various layers chosen for specific functions, the mechanical and shear separation properties of the substrate can be independently controlled. Figure 1 shows one of the possible configurations of this substrate. The characteristic features of this substrate configuration are:

1) It employs a Mo substrate core which can be thin enough to be flexible for use as a belt type substrate, or thick enough to be rigid.
2) A thin SiO_2 layer acts as a diffusion barrier preventing diffusion of impurities from the Mo substrate into the Si, and prevents any reaction between the substrate (core) and the silicon deposit. Because the Si-O bond is stronger than Mo-O bond, the integrity of SiO_2 on Mo is assured.
3) A thin Mo layer is deposited on top of the SiO_2 diffusion barrier. During silicon deposition, this will be converted into $MoSi_2$ and act as a shear separation interface.

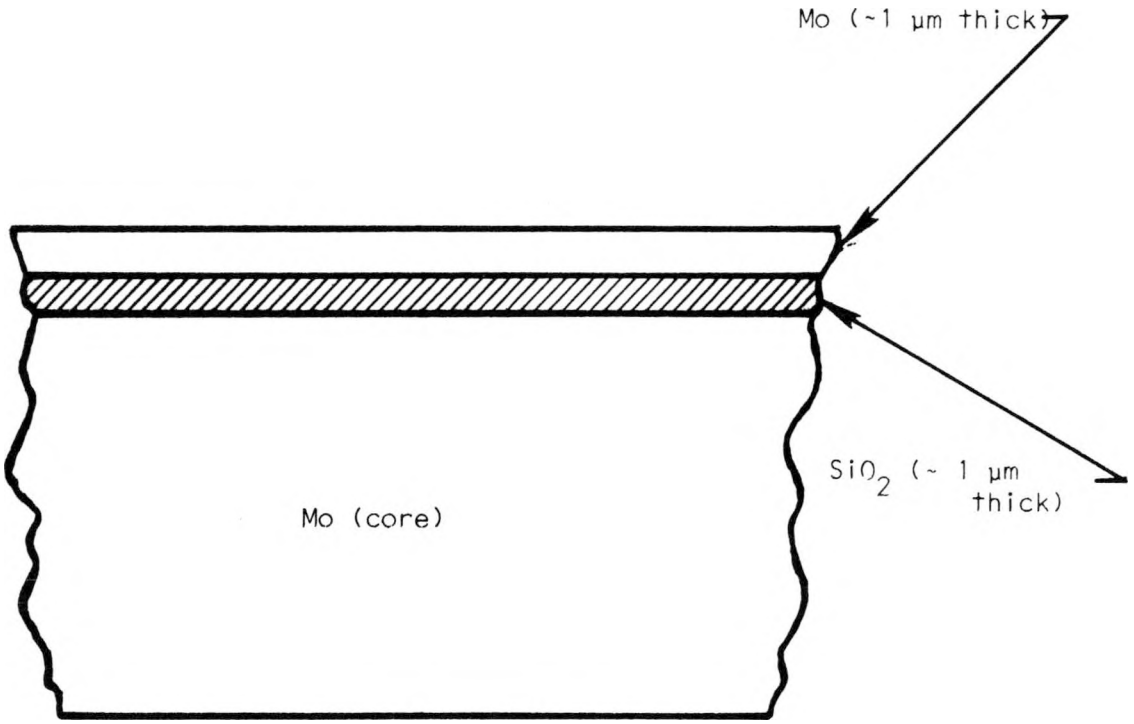

FIGURE 1: Schematic cross-section of a composite substrate utilizing SiO_2 diffusion barrier.

Composite substrates Mo (40 mils); SiO_2 (~1 μm): Mo (3000Å) have been fabricated, and shear separation has been successfully demonstrated. The thin SiO_2 layer was deposited by chemical vapor deposition from $SiCl_4$ and O_2 at 1150°C. The thin Mo film was deposited by sputtering.

As these composite substrates were re subjected to successive silicon deposition cycles, the $MoSi_2$ layer peeled off at a few small spots, exposing the (colored) oxide. Then, during a subsequent silicon deposition cycle, the silicon deposit adhered at the spots where the oxide was exposed. Thus, for complete recyclability of this composite substrate the $MoSi_2$ separation layer must be continuous and adherent to the oxide. Hence, optimizing the composite substrate parameters for $MoSi_2$-SiO_2 adherence is important.

A sample of a silicon ribbon separated from one of these composite substrates, with 10 μm etched from the surface, was submitted for Neutron Activation Analysis. It contained 0.39 ppm of Mo, which is comparable to the results obtained from ribbons separated from conventional Mo substrates and etched the same amount.

2.2 EXPERIMENTS WITH Al_2O_3 BARRIER LAYERS

Al_2O_3 has been used successfully as a diffusion barrier in semiconductor processing [2], and since it is a refractory material it is potentially promising as a barrier layer in making composite substrates. Mo substrates with 2500Å and 5000Å layers of Al_2O_3 were prepared by reactive sputtering. In both cases the Si ribbons sheared off. SEM photographs of the resulting substrate cross sections are similar in appearance to those formed on uncoated Mo substrates.

These layers, clearly evident in Figure 2, are presently being analyzed and are tentatively identified as silicide layers.

2.3 EXPERIMENTS WITH FINE POWDERY SILICON COATINGS

In the energy beam system, a fine powdery silicon is deposited in the cool exit end of the reaction tube. This has been collected and a slurry made from it with water. Mo substrates painted with the slurry produced good sheared ribbons. In order to test whether it was indeed a good release agent, an Al_2O_3 and a fused silica substrate were coated with the slurry, dried, and put through a deposition cycle. In both cases the deposited Si stuck to the substrates and shattered in cooling. Microscopic examination of the Si, through the clear quartz, showed no trace of the original brown colored silicon layer. It had apparently been densified during the deposition. With the Mo substrates therefore, a normal silicide layer was formed and standard shear separation took place.

2.4 EXPERIMENTS WITH RESURFACED SUBSTRATES

Two Mo substrates, which had been used for eight successive depositions, were surface ground. This removed all traces of silicide, exposing the bare substrate material. They were then used in repeated depositions with successful shearing taking place. This demonstrates that the bulk character of the Mo substrates is unaffected by repeated use.

2.5 EXPERIMENTS WITH CRYSTALLITE SIZE

In an attempt to determine if crystallite size in the Si ribbons depends on the crystallite size of the $MoSi_2$ layer, successive deposition

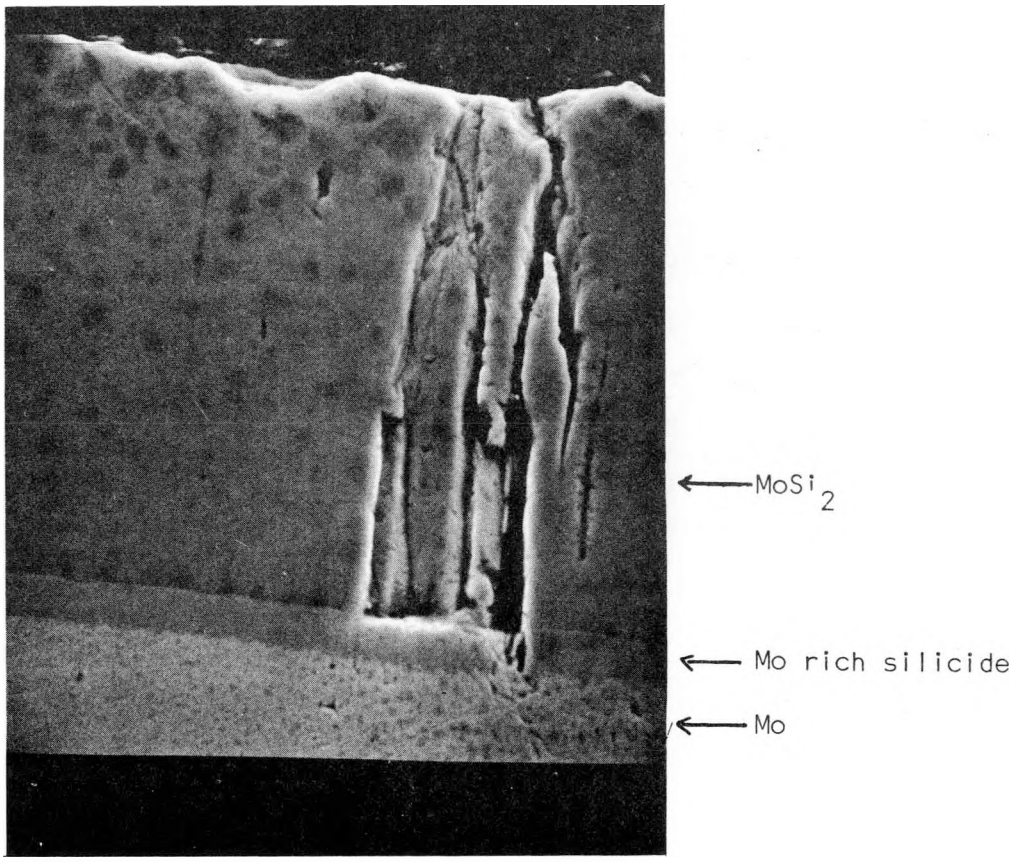

FIGURE 2
Cross-section of an Al_2O_3 coated Mo substrate after one silicon deposition cycle.

runs were made on a series of substrates. (The crystallite size in the $MoSi_2$ layer was found to increase with the number of deposition cycles. This can be clearly seen in the top surface views of $MoSi_2$ layers in reference 3.) Cross-sections were made of substrates used 1, 2, 3 and 4 times, and also of the Si ribbons grown on them. Figure 3 shows SEM photographs of the substrates used 1 and 4 times. Figure 4 shows the ribbons grown on these substrates. The sections were treated with BF etch to show grain structure. Although the grain size of Si from the substrate used 4 times seems slightly larger, it did not seem significant enough to pursue further.

2.6 MOLYBDENUM INCORPORATION MECHANISMS

By various analytical techniques such as SIMS and NAA, we had determined that the back surfaces (the surfaces in contact with the Mo substrates) of the separated silicon ribbons were contaminated by Mo at the trace levels (in the ppm range)[3]. Molybdenum at these concentration levels was found to seriously degrade the performance of silicon solar cells[4]. However, by etching off about 25 μm from the backside of the silicon ribbons, Mo concentration was reduced to below the detection limit (~0.1 ppm) of NAA. It would be desirable to minimize the amount of silicon to be etched off for reducing the Mo contamination.

The possibilities by which silicon films can be contaminated by Mo substrates are:

1. Chloride Transport: Mo can react with chlorine (from SiH_xCl_{4-x} or HCl in the silicon deposition ambient) to form gaseous chlorides which can be reduced to Mo and get incorporated into the growing silicon film. To test this possibility we have used thermal decomposition of SiH_4 for silicon deposition. The Mo level in these silicon ribbons

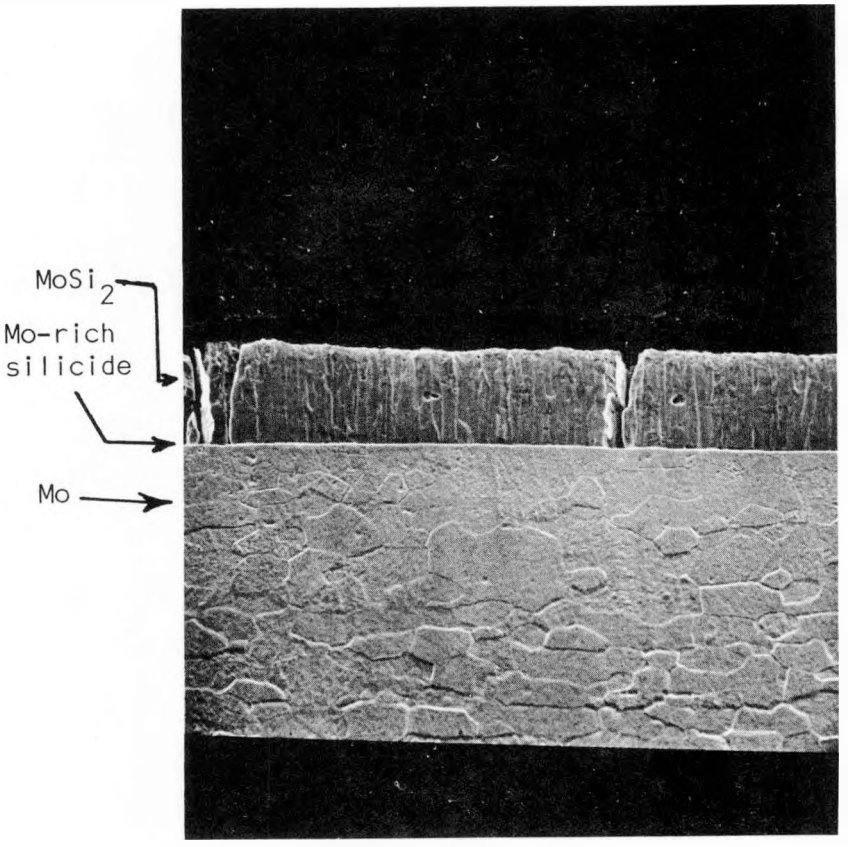

SUBSTRATE CROSS-SECTION
USED 1 TIME 320X

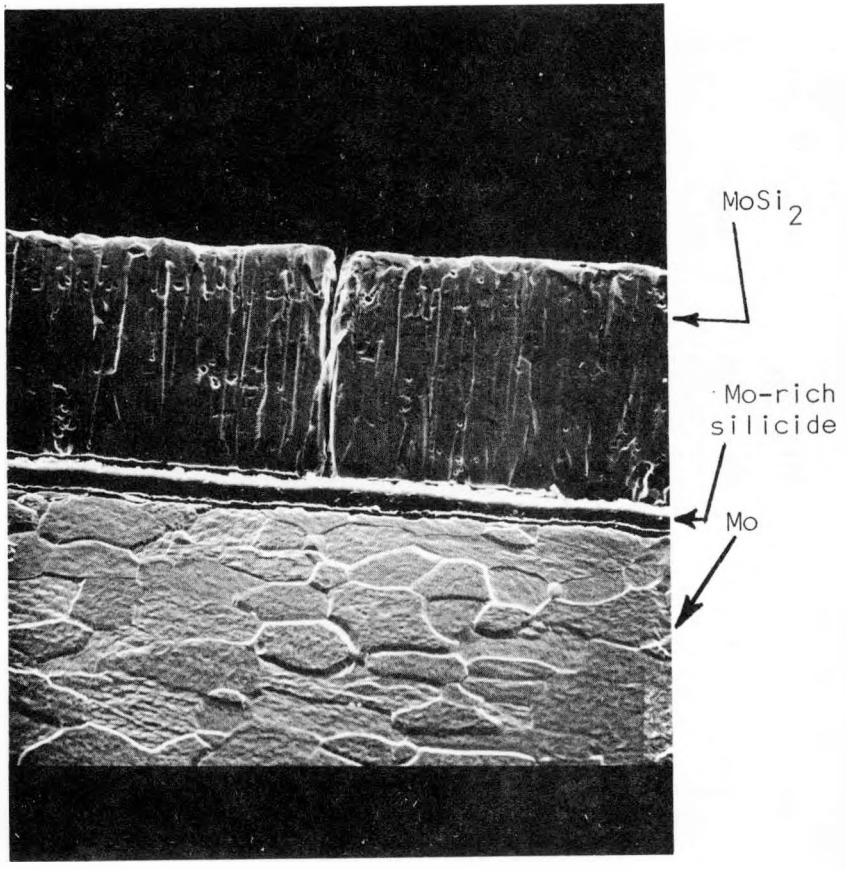

SUBSTRATE CROSS-SECTION
USED 4 TIMES 320X

FIGURE 3

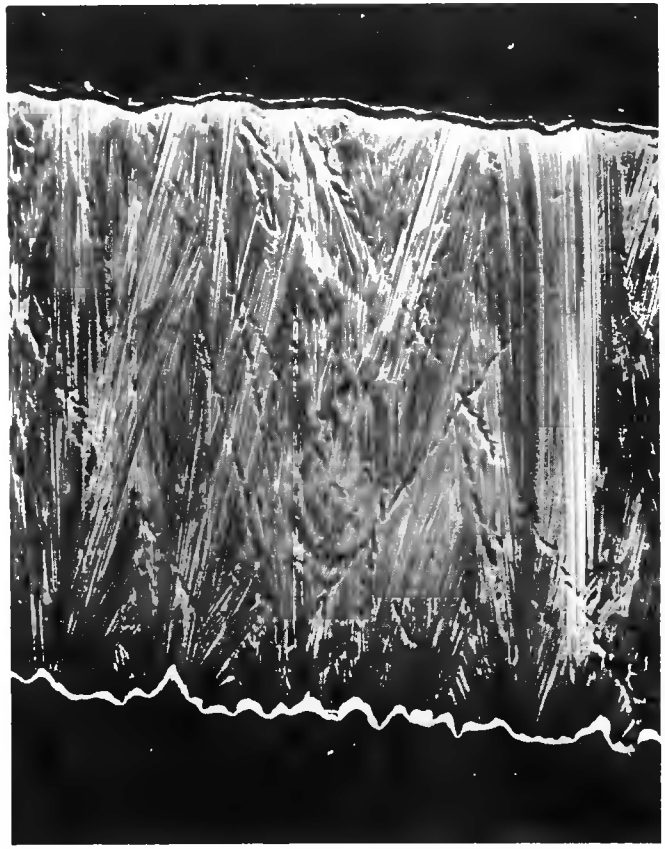

CROSS-SECTION OF
SILICON RIBBON FROM
SUBSTRATE USED 1 TIME
320X

CROSS-SECTION OF
SILICON RIBBON FROM
SUBSTRATE USED 4 TIMES
320X

FIGURE 4

was found (as determined by NAA) to be about the same as in ribbons produced by the hydrogen reduction of $SiHCl_3$ or $SiCl_4$. Even though this does not rule out the chloride transport mechanism completely, it does indicate that this is not a dominant mechanism.

2. Bulk Diffusion of Mo: This is not considered to be important, because it has been shown in the literature [5] that silicon is the dominant diffusing species in the formation and growth of $MoSi_2$ between Mo and Si layers.
3. Grain Boundary Diffusion of Mo: This can be very important since grain boundary diffusion coefficients can be orders of magnitude higher than bulk diffusion coefficients. We have not yet tested this possibility experimentally.
4. Imperfect Shear Separation: This is another important possibility. Shear separation appears to occur in the silicon film very close to the $MoSi_2$-Si interface. However, if the shearing were not perfect and occurred at randomly isolated regions slightly into the $MoSi_2$ layer near the $MoSi_2$-Si interface, it could account for the trace level Mo contamination at the back side of the silicon films. We examined the back side of separated silicon films for the presence of isolated $MoSi_2$ particles in an SEM with an energy dispensive x-ray unit and found no operating mechanism, or that the $MoSi_2$ particle size is below the detection capabilities of the SEM.

3.0 ENERGY BEAM DEPOSITION (EBD)

3.1 DEPOSITION PARAMETRIC STUDIES

The parametric studies of EBD have continued during this quarter and in the following the results of these studies to date are summarized.

The effect of input $SiHCl_3$ concentration (given as $\frac{Cl}{H}$ ratio) on the efficiency of deposition (calculated from weight gain measurements) is shown in Figure 5. In these experiments, the total gas flow rate, RF power of the plasma and the substrate temperature were maintained constant at 25 LPM, 2.5 kW and 1150°C respectively. The solid curve shows the calculated efficiency when equilibrium in the gas phase is assumed [6]; i.e. this curve indicates the maximum possible efficiency obtainable in a conventional CVD process at 1150°C, using $SiHCl_3$. When compared to the equilibrium curve, the average EBD efficiencies were higher by a few percent (0 to 5%) for $\frac{Cl}{H}$ ratios < 0.12, and lower by a few percent for $\frac{Cl}{H}$ ratios >0.12. In best individual runs, deposition efficiencies are higher by up to 12% compared to the equilibrium efficiency.

Figure 6 shows the effect of total gas flow rate on the deposition efficiency for horizontal and vertical orientations of the EBD system when the input $\frac{Cl}{H}$, RF power of the beam, and the substrate temperature were maintained constant at 0.1, 2.5 kW and 1150°C respectively. For a given flow rate, the efficiency in a vertical configuration was lower than in a horizontal configuration by upto 7%. However, in both cases efficiency decreased with increase in flow rate. Deposition rate in μm/min was calculated from the thickness of the separated silicon films.

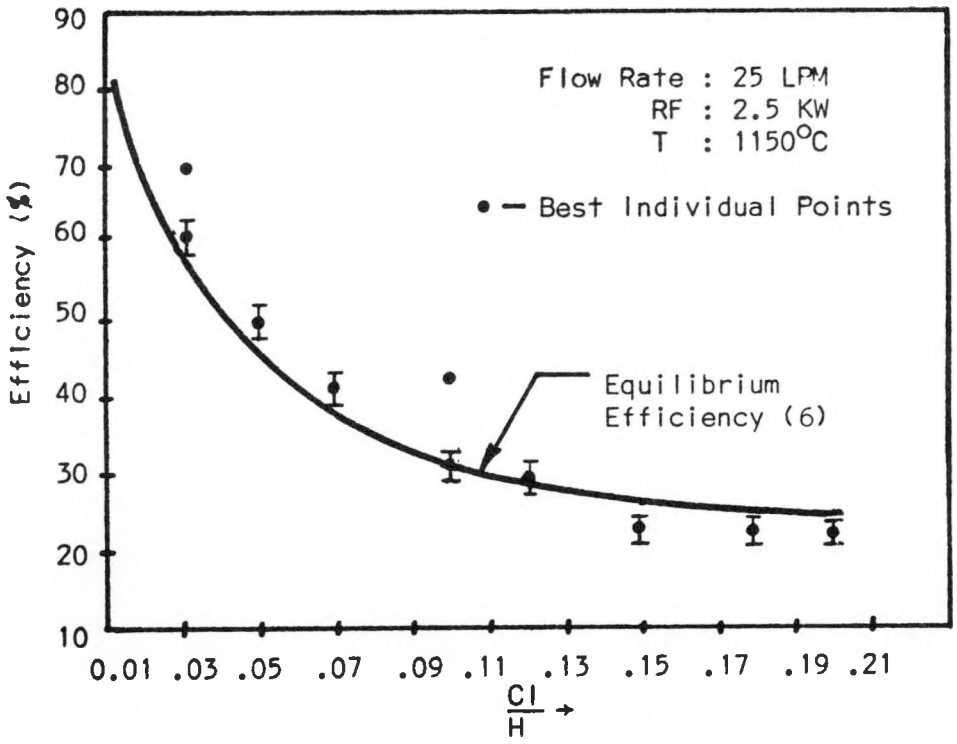

Figure 5: Effect of $SiHCl_3$ Concentration on Efficiency in Horizontal EBD.

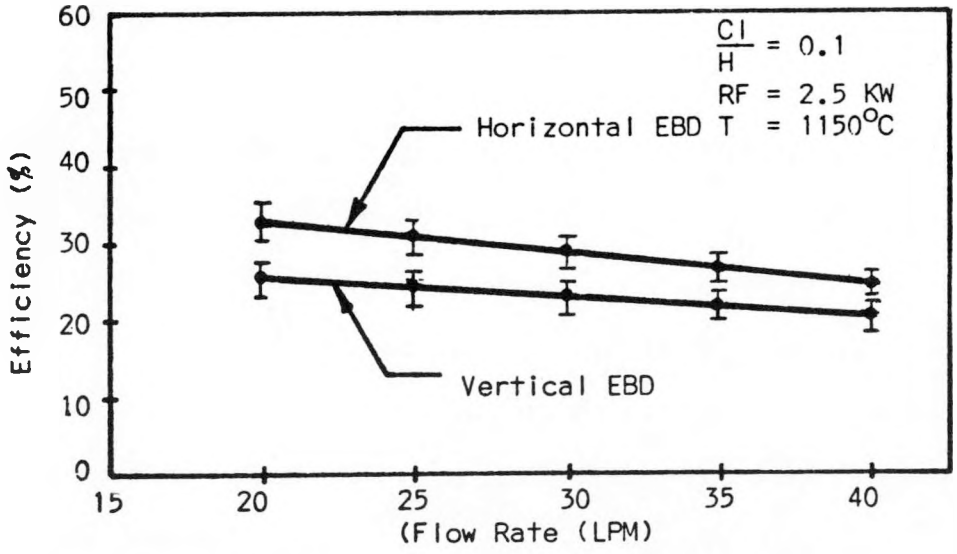

Figure 6. Effect of Flow Rate on Efficiency

Figure 7 shows a typical deposition rate profile along the center line of the substrate. This profile was obtained with a total gas flow rate of 25 LPM, $\frac{Cl}{H}$ ratio of 0.1, B_2H_6 (10 ppm in H_2) flow of 0.24 LPM, RF power of 1.5 kW and a substrate temperature of 1150°C. The deposition rate increases rapidly and reaches a maximum about 5" from the beginning of the deposition zone, and then decreases. Maximum deposition rates of up to 16 μm/min. were realized in some experiments. This kind of deposition rate variation along the deposition zone is not detrimental to the production of uniformly thick silicon ribbons, since a continuous EBD system is envisioned to be the eventual mode of operation. In a continuous EBD system, the substrates will be translated through the deposition zone, which will average out the deposition rate, and silicon ribbons of uniform thickness will result. Deposition rate across the width of the substrates was found to vary slightly, indicating non-uniform mass transfer effects at the corners of the square cross-section reactor. This thickness variation across the width of the ribbon is sufficiently small that it does not affect the efficient use of this material for solar cell processing. The deposition rates on the bottom, side and top substrates in the horizontal EBD system were very similar and thus no definitive effects of gravity were observed in the horizontal system.

RF power of the beam did not directly appear to affect its deposition efficiency or deposition rate, except through its effects on the temperature of the deposition zone [1]. Substrate temperature plays a role in the shear separation process as well as the deposition process. For reliable shear separation of the silicon ribbon from molybdenum substrates, it was found [3] that the deposition temperature should be at least 1100°C. Hence most of the experiments to date were performed with a deposition temperature between 1100 and 1200°C.

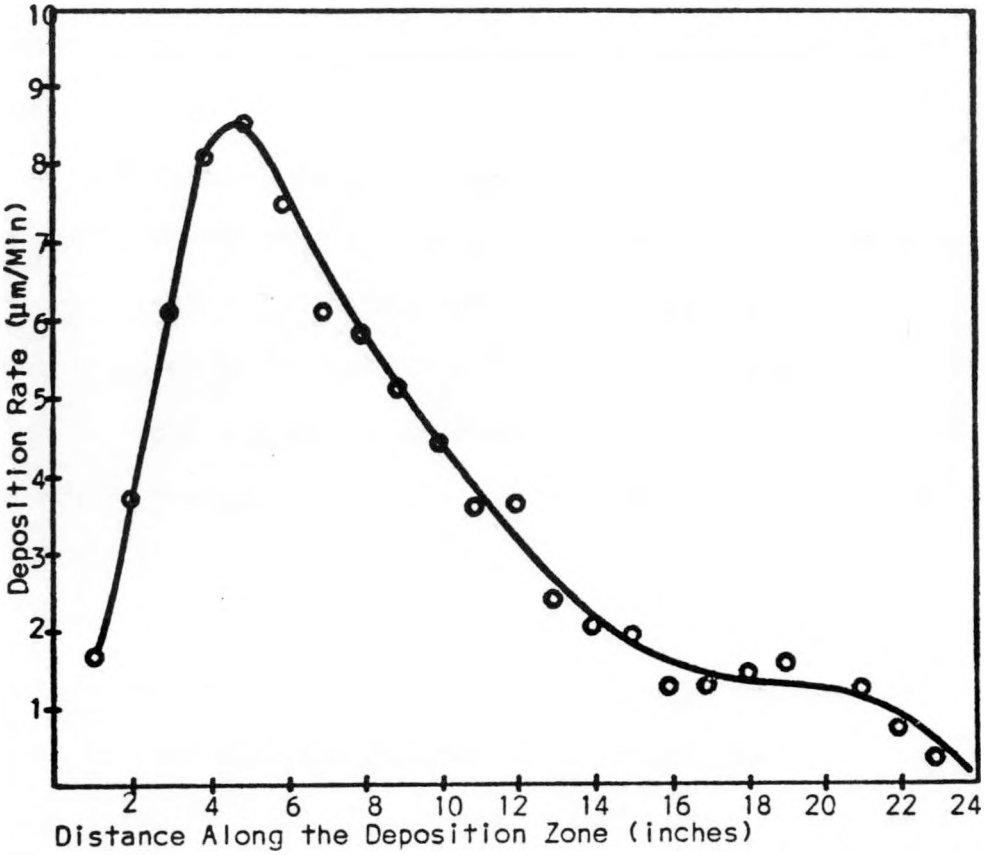

Figure 7: Typical Deposition Rate Variation Along the Center Line of the Substrate.

In this range, deposition efficiency, deposition rate, and deposit morphology were not found to be temperature sensitive. However, recently we have observed that dense silicon films can be deposited by EBD at as low a temperature at 900°C, and can be successfully separated from the substrate by annealing at 1200°C for 30 minutes before cool down. We plan to characterize the low temperature EBD process for deposition efficiency, deposition rate and deposit quality.

3.2 EFFICIENCY OF DEPOSITION

Even though chemical equilibrium calculations for a plasma temperature in the neighborhood of 4300 K indicate [6] that over 95% of the input $SiHCl_3$ is reduced to silicon vapor for the concentration range shown in Figure 5, experimental EBD efficiencies are found to be strongly dependent on concentration. Furthermore, the average EBD efficiency is only a few percent different from what it calculates to be when complete equilibrium is established in the gas phase at the deposition temperature of 1150°C (the EBD efficiency being higher than the equilibrium efficiency for $\frac{Cl}{H} < 0.12$ and lower for $\frac{Cl}{H} > 0.12$, Figure 5). Gas phase nucleation and powder growth can partly account for the lower than expected efficiencies. Homogeneous nucleation of silicon and subsequent powder growth during EBD were inferred from the brown powdery deposits at the exit side of the deposition chamber and the exhaust pipe. Thus, lower than expected EBD efficiency values are partly due to small silicon particles being exhausted from the reactor instead of being incorporated into the growing silicon ribbon. The same phenomenon can explain why the deposition efficiencies in the vertical system are lower than in the horizontal system. In a vertical system in which the gases are introduced at the top and exhausted at the bottom, silicon particles (since their density is higher than that of the ambient gases), can

travel through the deposition zone more quickly and thus suffer fewer collisions with the substrate surface. This will result in more of the silicon particles being exhausted from the reactor, thus resulting in lower efficiency than in a horizontal EBD system.

An important factor that determines the deposition efficiency using a high temperature plasma is the rapidity with which the plasma is quenched to a low temperature [7,8]. For example, in hydrogen reduction of Ta_2O_5 to produce Ta metal using a high temperature plasma jet, deposition efficiency was increased from 15% to 42% by decreasing the quenching distance from 5" to $\frac{1}{2}$" [8]. Similar results were reported in the reduction of other refractory metal oxides such as WO_3. We have obtained similar results in some preliminary experiments involving gas chromatographic (GC) analysis of the exhaust gases from the EBD reactor. Regular EBD runs were conducted, except that the furnace was not used to heat the substrates. Deposition efficiency was calculated from the concentration of the exhaust gases determined by GC analysis. In the range of concentrations investigated ($0.04 \leq \frac{Cl}{H} \leq 0.1$), efficiencies in excess of 50% were observed. These studies will be continued to determine the effects of quenching on deposition efficiencies for higher $\frac{Cl}{H}$ ratios.

3.3 WHISKER AND NODULE GROWTH IN EBD

In the previous quarterly report [1] we reported on the growth of whiskers and nodules during EBD, and discussed the possible mechanisms for their growth. During this quarter, we have further characterized whiskers and the deposition conditions leading to their growth.

The whisker tips and nodules were examined by electron probe x-ray micro-analysis, and no impurities were detected. This will

certainly rule out the VLS (impurity) mechanism for whisker growth in EBD. The possibility of a stress relief mechanism was also examined. Substrate temperature was monitored during a silicon deposition run. Substrate temperature was found to increase gradually by about 15°C and stabilize during the run. This will introduce tensile stresses in the silicon film, because the thermal expansion coefficient of silicon is smaller than that of Mo. However, for hillock (whisker) growth the silicon film should be under compression [1]. Furthermore, the temperature change after the initiation of deposition is so small that it cannot generate stresses high enough to cause silicon to flow. Thus a stress relief mechanism does not appear to be responsible for whisker growth in EBD.

The deposition chamber geometry appears to influence whisker and nodule growth. When a square cross-section reactor (with a circular expanded entry section to minimize the propensity for beam arcing) was employed, numerous whiskers and nodules almost always resulted. With a circular cross-section reactor (with circular expanded part for minimizing beam arcing), nodule and whisker density was dramatically reduced. When deposition was conducted with a rotating nozzle in a circular cross-section reactor, a few nodules were observed, but whiskers were totally absent.

In experiments employing the expanded deposition chamber for arc minimization, a brown powdery silicon deposits at the neck of the expanded portion of the quartz chamber. We believe that one of the operating mechanisms for whisker and nodule growth during EBD is by dislodgement of these powdery silicon particles (by the flowing reactant gas stream) and their subsequent landing on the dense silicon

film growing on the Mo substrates. When the particles land on the growing silicon film with a favorable orientation, whisker growth can occur by a self-perpetuating re-entrant twin mechanism. When orientation is not favorable, these particles result in nodular growth. The substantial difference in density of nodules and whiskers in the silicon films obtained from square and circular cross-section reactors is due to the fact that particles from the deposit at the expanded neck of the square cross-section reactor can be dislodged more easily than those in the neck of the round cross-section reactor. In the deposition experiments with a rotating nozzle, this situation (powdery deposit and subsequent dislodgement of particles) did not occur. We plan to continue characterization of whisker and nodule growth during EBD to determine additional operative mechanisms.

3.4 ROTATING NOZZLE DEPOSITION

The modified rotating energy beam nozzle with reduced electrode offset (shown in the Appendix) has been fabricated and tested for silicon deposition on the electrode tip. Problems were encountered while using this nozzle in tuning the impedance matching network for efficient operation of the energy beam. With this rotating nozzle, the plasma could not be sustained for RF powers less than 3.0 kW, whereas with the conventional nozzle, as low as 1000 watts of RF power was found to be sufficient to maintain a stable plasma beam with identical gas flow rates. When a 3.0 kW rotating beam was employed during silicon film formation, silicon deposition was observed on the tungsten electrode as well as on the boron nitride housing of the nozzle, due to the excessively high temperatures in these areas.

The problem in tuning the impedance matching network while using the rotating nozzle is due to the impedance of the rotating assembly [1] being considerably different from that of the conventional nozzle. We have designed and fabricated a new rotating assembly, a schematic of which is shown in Figure 8. In this new assembly, the (massive) rotating conducting feed-through in the old assembly [1] is replaced by a high dielectric strength elastomer (spring loaded) dynamic seal obtained from Fluorocarbon Co., Los Alamitos, California 90720. The seal retainer was made out of Macor (trade name of Corning for a machinable glass ceramic with a high dielectric strength) to minimize the potential for arcing near the seal. This assembly is currently being tested.

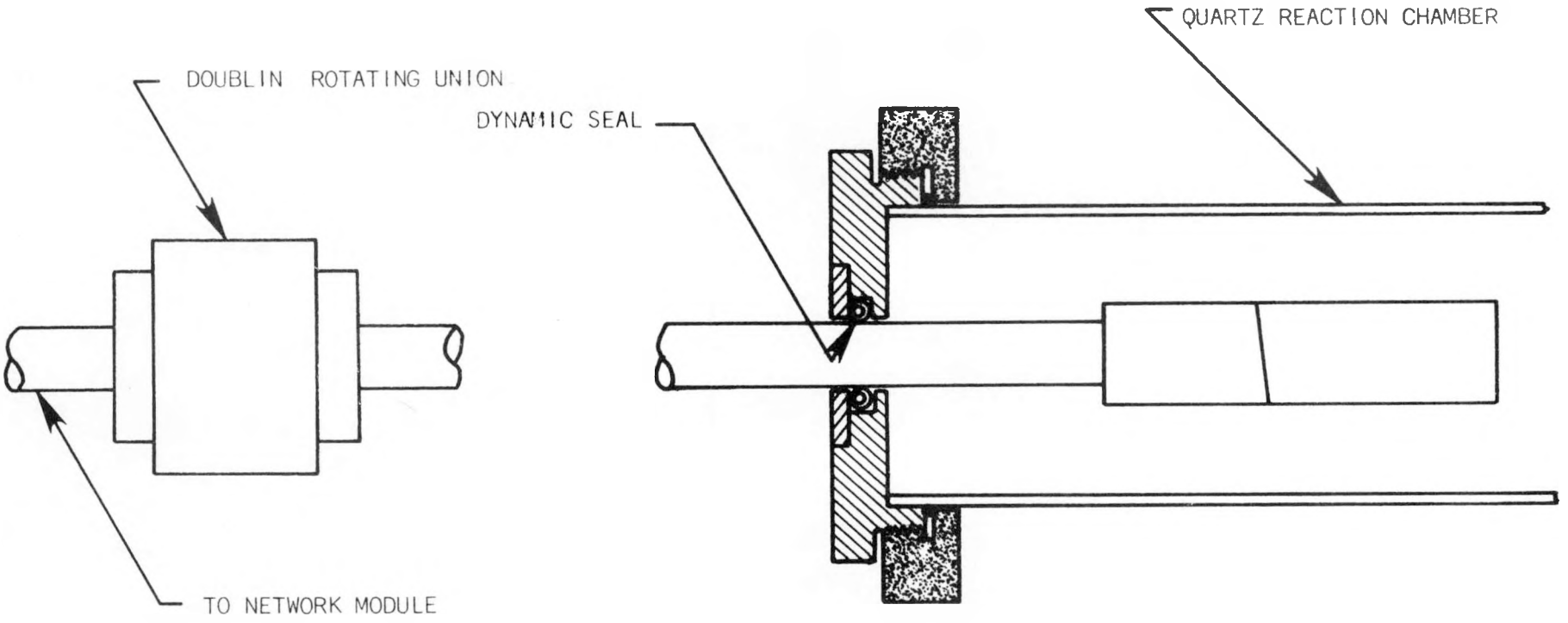

FIGURE 8: Modified Rotating Nozzle Assembly

4.0 GRAIN SIZE ENHANCEMENT

In the last quarterly [1] we reported that possible profile furnace contamination during RTR grain enhancement was resulting in unmeasurably low diffusion lengths (determined by the SPV technique) in grain-enhanced EBD silicon films. To verify this we have grain enhanced some pre-etched (to remove about 10 μm from each surface to minimize the Mo level) EBD ribbons without a profile furnace at a rate of 1 cm per minute. These grain enhanced EBD ribbons have exhibited diffusion length in the range of 5 - 15 μm.

When the grain enhanced EBD films were gettered by a process involving a double-sided phosphorous diffusion at 900°C, minority carrier diffusion lengths ranging up to 75 μm resulted. (One of the n+ layers from the n+-p-n+ structure, formed by the double sided diffusion was etched off and diffusion lengths were measured by OCPV using the n+-p junction as the barrier.)

Recently, profile furnace contamination problems during RTR grain enhancement appear to have been substantially reduced. Hence we are now planning to grain enhance EBD ribbons at high rates in the RTR apparatus with the profile furnace, and to characterize them for minority carrier diffusion length.

5.0 SOLAR CELL FABRICATION AND EVALUATION

Pre-etched EBD silicon ribbons were grain enhanced and processed into 1 x 2 cm solar cells. Because of some chipping at the edges of the ribbon during processing, some of the cells ended up with area somewhat less than 2 cm^2. The processing sequence employed is as follows:

1. HF dip and rinse
2. Clean in $H_2SO_4 + H_2O_2$ at 120°C, rinse, blow dry
3. PH_3 diffusion at 900°C for 18 minutes.
4. Establish a mesa pattern on one side by photoresist masking
5. Etch in a $CF_4 - O_2$ plasma
6. Low pressure CVD (750°C, 30 min) for an 850Å thick Si_3N_4 AR coating
7. Open contact finger pattern in the Si_3N_4 by photoresist masking
8. Metallize front and back by sequential Pd:Ag plating.

Figure 9 shows an example of a fabricated cell. Figure 10 shows the I-V characteristic of this cell (991A-2) under ELH simulated AM1 conditions (100 mW/cm^2). This cell had an area of 2 cm^2 and exhibited a conversion efficiency of 9.6% with V_{OC} = 0.54V, J_{SC} = 28.5 mA/cm^2 and FF = 62%. Figure 11 shows the I-V characteristic of another cell (991A-1). This has an area of 1.65 cm^2 and a conversion efficiency of 10.06% with V_{OC} = 0.54, J_{SC} = 29.5 and FF = 63%.

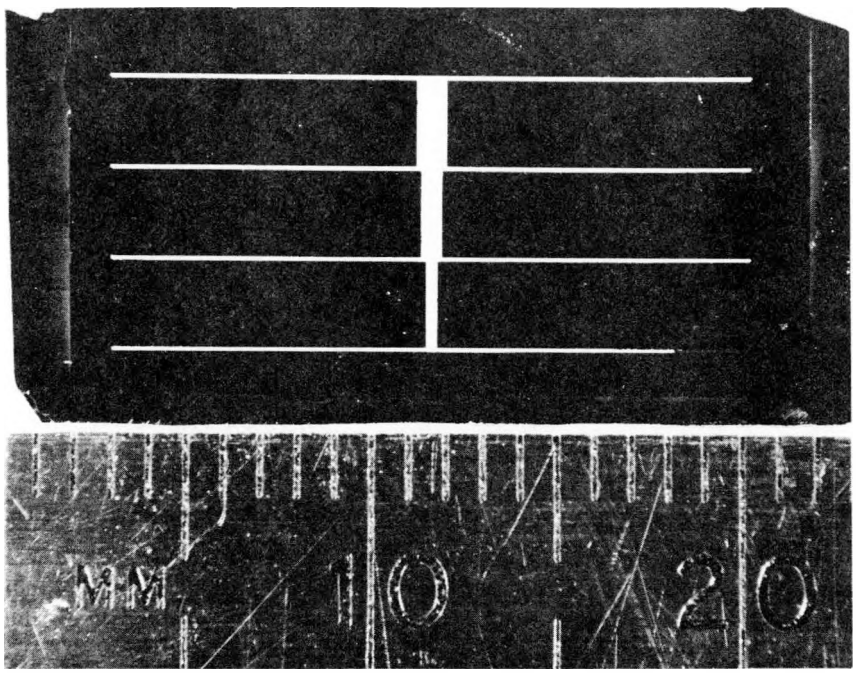

FIGURE 9: Photograph of a typical solar cell fabricated during this quarter.

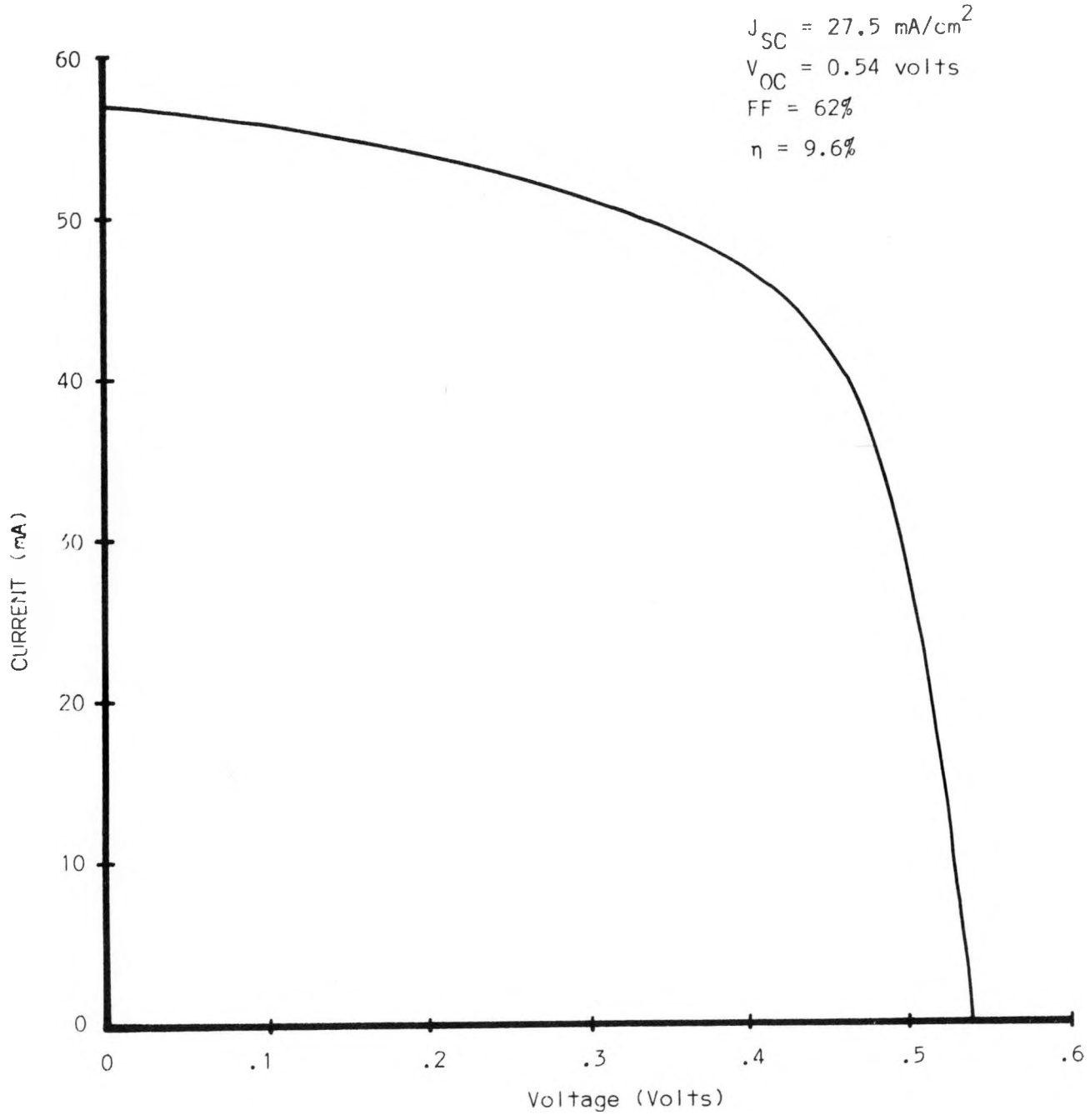

FIGURE 10: I-V characteristic of the cell 991A-2, under AM1 illumination.

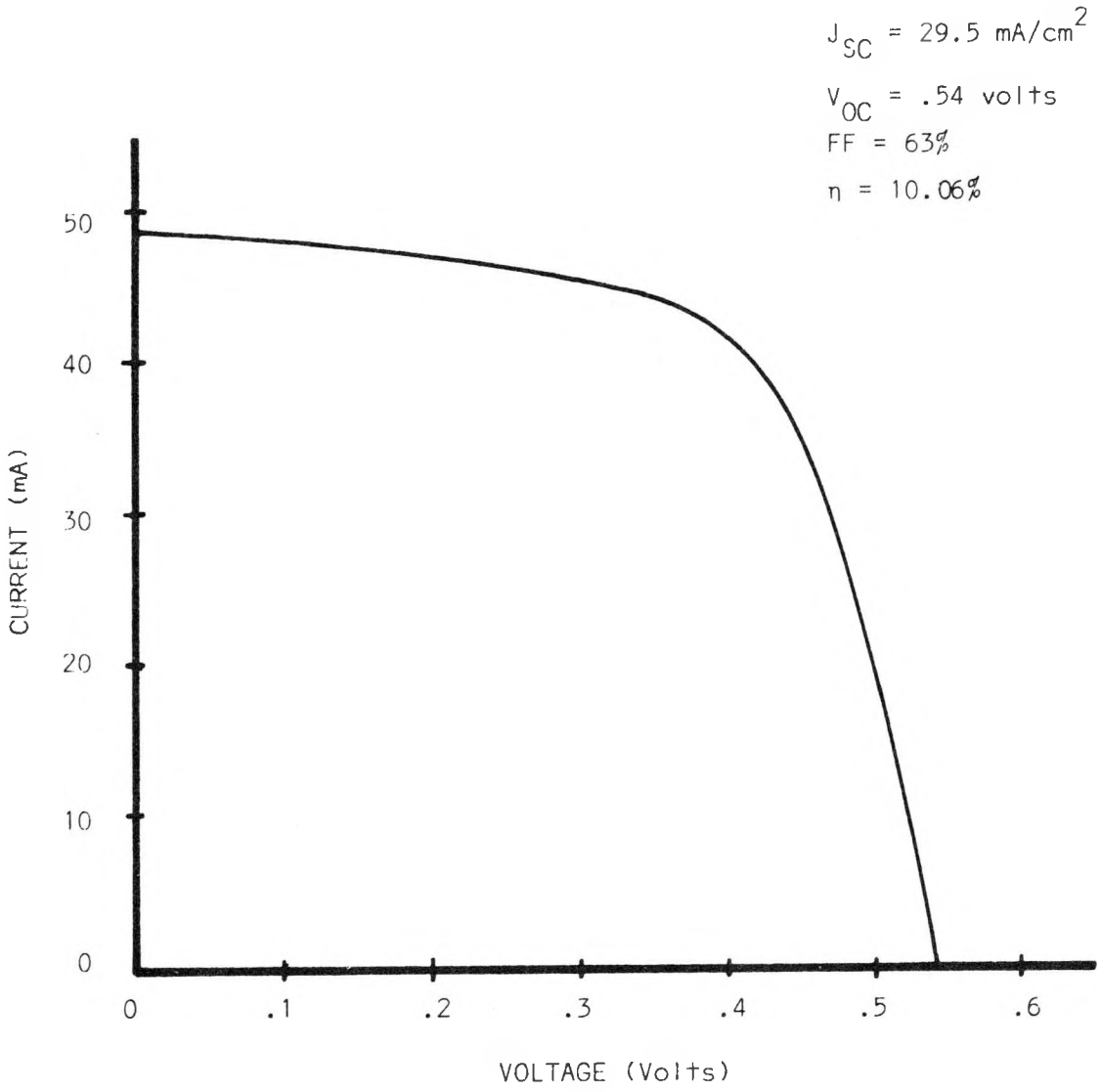

FIGURE 11: I-V characteristic of the cell 991A-1, under AM1 illumination.

6.0 PLANS FOR NEXT QUARTER

During the next quarter we plan to:

- Continue evaluation of composite TESS substrates
- Test the new rotating nozzle assembly for its effectiveness in minimizing impedance matching problems, and evaluate its deposition characteristics
- Complete designing the continuous EBD system and initiate fabrication
- Routinely grain enhance EBD silicon films by the RTR technique, fabricate solar cells and evaluate their performance.

REFERENCES

1. K. R. Sarma et. al, Thin Film Polycrystalline Silicon Solar Cells, Quarterly Report No. 1, DOE Contract No. ET-78-C-03-2207, Jan. 1979.
2. I. A. Aboaf, J. Electrochem. Soc., 114, 948 (1967)
3. K. R. Sarma et. al., Thin Films of Silicon on Low-Cost Substrates, Final Report, DOE Contract No. EY-76-C-03-1287, (1978)
4. R. H. Hopkins et. al., Effect of Impurities and Processing on Silicon Solar Cells, JPL Contract No. 954331, Technical Quarterly Report, March 1978.
5. G. J. Van Gurp, in Semiconductor Silicon, Eds. H. R. Huff and E. Sirtl, 342, (1977)
6. K. R. Sarma et. al., Proc. 13th IEEE Photovoltaic Specialists Conference, 466, (1978)
7. C. S. Stokes, in Reactions Under Plasma Conditions, Vol. 2, Ed. M. Venugopalan, Wiley-Interscience, New York, 259, (1971)
8. C. S. Stokes, in Chemical Reactions in Electrical Discharges, Adv. in Chem. Series, ACS, 390, (1969)

APPENDIX

REVISIONS					
REV.	ECO NO.	CHANGE	DATE	BY	ENGR

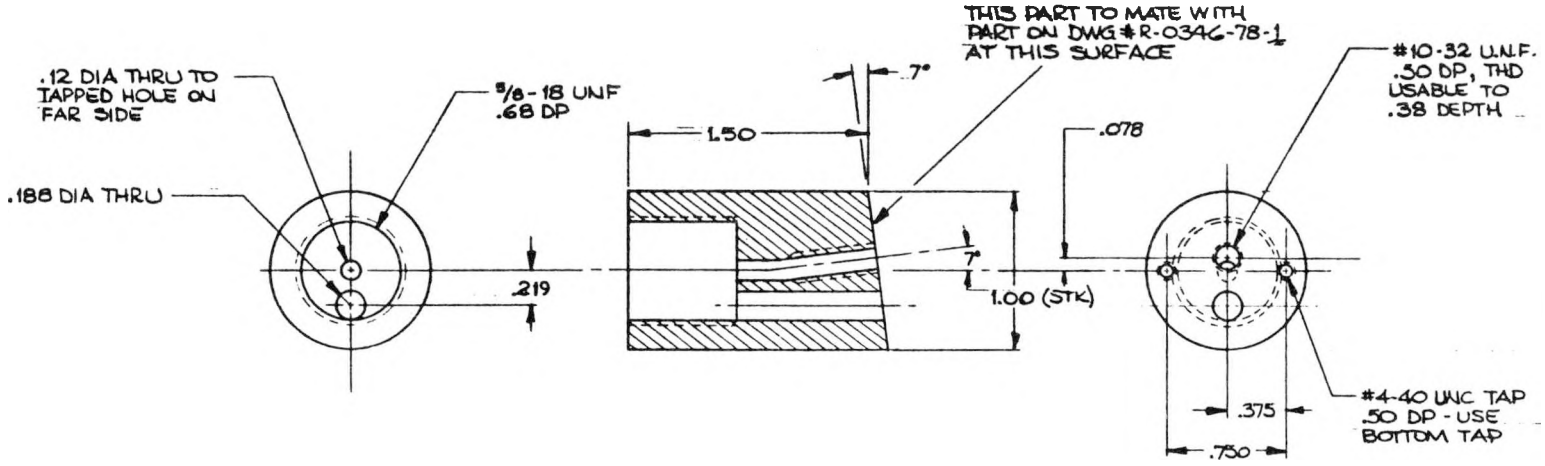

UNLESS OTHERWISE SPECIFIED, TOLERANCES:
INCHES .XX ± .02 .XXX ± .005
MILLIMETERS .X ± .XX ±
ANGULAR ± 1°
63/ RMS ALL MACHINED SURFACES
FEATURE CONTROL SYMBOLS PER ANSI Y14.5
BREAK ALL SHARP EDGES AND CORNERS, REMOVE BURRS.
UNDERLINED DIM NOT TO SCALE
THIRD ANGLE ORTHOGRAPHIC PROJECTION IS USED

MATERIAL: MOLYBDENUM
HEAT TREAT:
APPLIED FINISH:
DRAWN BY: F.J. MOSNA — DATE: 12-21-78
CHECKED BY: — DATE:
ENGR APPROVAL: — DATE:

MOTOROLA INC.
Discrete Semiconductor Division

TITLE: E-BEAM NOZZLE CONNECTOR

SIZE: C | CODE IDENT. NO.: 04713 | DRAWING NO.: R-0346-78-2
SCALE: 2X | WEIGHT: | SHEET 2 OF 2